Catalase and *NO CATALASE ACTIVITY1* Promote Autophagy-Dependent Cell Death in *Arabidopsis*[CW][OPEN]

Thomas Hackenberg,[a] Trine Juul,[a] Aija Auzina,[a] Sonia Gwiżdż,[a] Anna Małolepszy,[a] Katrien Van Der Kelen,[b,c] Svend Dam,[a] Simon Bressendorff,[d] Andrea Lorentzen,[e] Peter Roepstorff,[e] Kåre Lehmann Nielsen,[f] Jan-Elo Jørgensen,[a] Daniel Hofius,[d,g] Frank Van Breusegem,[b,c] Morten Petersen,[d] and Stig Uggerhøj Andersen[a,1]

[a] Department of Molecular Biology and Genetics, Aarhus University, DK-8000 Aarhus C, Denmark

[b] VIB Department of Plant Systems Biology, Ghent University, B-9052 Ghent, Belgium

[c] Department of Plant Biotechnology and Bioinformatics, Ghent University, B-9052 Ghent, Belgium

[d] Department of Biology, University of Copenhagen, DK-2200 Copenhagen N, Denmark

[e] Department of Biochemistry and Molecular Biology, University of Southern Denmark, DK-5230 Odense M, Denmark

[f] Department of Biotechnology, Chemistry and Environmental Engineering, Aalborg University, DK-9000 Aalborg, Denmark

[g] Department of Plant Biology and Forest Genetics, Swedish University of Agricultural Sciences and Linnean Center for Plant Biology, Uppsala BioCenter, 75007 Uppsala, Sweden

Programmed cell death often depends on generation of reactive oxygen species, which can be detoxified by antioxidative enzymes, including catalases. We previously isolated catalase-deficient mutants (*cat2*) in a screen for resistance to hydroxyurea-induced cell death. Here, we identify an *Arabidopsis thaliana* hydroxyurea-resistant autophagy mutant, *atg2*, which also shows reduced sensitivity to cell death triggered by the bacterial effector avrRpm1. To test if catalase deficiency likewise affected both hydroxyurea and avrRpm1 sensitivity, we selected mutants with extremely low catalase activities and showed that they carried mutations in a gene that we named *NO CATALASE ACTIVITY1* (*NCA1*). *nca1* mutants showed severely reduced activities of all three catalase isoforms in *Arabidopsis*, and loss of NCA1 function led to strong suppression of RPM1-triggered cell death. Basal and starvation-induced autophagy appeared normal in the *nca1* and *cat2* mutants. By contrast, autophagic degradation induced by avrRpm1 challenge was compromised, indicating that catalase acted upstream of immunity-triggered autophagy. The direct interaction of catalase with reactive oxygen species could allow catalase to act as a molecular link between reactive oxygen species and the promotion of autophagy-dependent cell death.

INTRODUCTION

Programmed cell death (PCD) is a necessary part of the life of multicellular organisms. It is associated with normal development and with immune responses aimed at pathogen clearance and destruction of otherwise harmful cells. Plant and animal innate immune systems detect conserved microbe-associated molecular patterns, such as flagellin-derived peptides, using pattern recognition receptors (Ausubel, 2005). To circumvent this detection system, adapted plant pathogens inject effectors directly into plant cells. In resistant plants, plant immune receptors known as R proteins detect the presence of effectors. This recognition leads to effector-triggered immunity, which often culminates in a hypersensitive response (HR) leading to accumulation of reactive oxygen species (ROS) and PCD (Jones and Dangl, 2006).
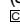
Since the discovery more than two decades ago of HR-associated ROS accumulation (Doke, 1983), also known as the oxidative burst, its causal relationship with PCD has been an active area of research. Over the years, evidence has accumulated that ROS trigger PCD and are not merely cell death by-products. For instance, pharmacological treatments with ROS antagonists block induction of HR-associated PCD (Lamb and Dixon, 1997), transgenic plants with lower levels of antioxidative enzymes display aggravated PCD responses (Van Breusegem and Dat, 2006), and superoxide induces runaway cell death in *Arabidopsis thaliana lesions simulating disease resistance1* mutants (Jabs et al., 1996). These observations highlight the importance of understanding how the plant interprets ROS signaling to induce PCD. Modulation of ROS levels during a HR could result in oxidative modification of countless proteins, emphasizing the complex nature of this topic and the potential difficulties in characterizing the nature of the ROS signal that induces PCD.
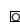
Since ROS signaling events resulting in PCD occur downstream of pathogen effector recognition by plant R proteins, genetic identification of signaling components required for R protein–dependent PCD is one possible avenue of investigation. It was revealed that autophagy components are involved in PCD execution downstream of the R protein RPM1 using an avrRpm1-expressing strain of the hemibiotrophic bacterium *Pseudomonas syringae* pv *tomato* (*Pst*) in a reverse genetics approach (Hofius et al., 2009). Furthermore, accumulating evidence suggests the existence of autophagy-dependent cell death pathways across the eukaryotic kingdom (Hofius et al., 2011). Autophagy facilitates

catabolism of cellular components and requires the action of autophagy-related genes (*ATG*) that coordinate membrane rearrangements (Mizushima, 2007). It comprises both unselective bulk degradation of cytoplasmic contents and selective autophagy of specific organelles or proteins. In *Arabidopsis*, selective autophagy is mediated by the recently identified cargo receptor NEXT TO BRCA1 GENE1 (NBR1), which is itself degraded in the vacuole upon increased autophagic activity (Svenning et al., 2011).

In addition to autophagic components, metacaspases also play an important role in execution of cell death triggered by RPM1 (Coll et al., 2010). Furthermore, a diverse group of PCD signaling components, including an leucine-rich repeat kinase, an Asp protease, and a uridine diphosphate-glucosyl transferase, seems to operate downstream of another R protein from *Arabidopsis*, RPP4 (Wang et al., 2011). In tomato (*Solanum lycopersicum*), E3 ubiquitin ligases were required for PCD downstream of Cf-9 (González-Lamothe et al., 2006). However, none of the PCD signaling components identified so far appear to be directly associated with ROS, and it remains an open question how ROS signaling induces PCD in plants.

Originally aimed at understanding the mechanisms of PCD induced by the antineoplastic drug hydroxyurea, we conducted a forward genetic screen for hydroxyurea resistance in *Arabidopsis*. The screen appeared to select specifically for mutants with compromised activity of the antioxidative, hydrogen peroxide (H_2O_2)–decomposing enzyme catalase, as we recovered 17 independent *cat2* mutant alleles. We showed that hydroxyurea and catalase interacted directly, indicating that catalase was involved in drug toxification and offering a likely explanation for the catalase specificity of the screen (Juul et al., 2010).

Here, we describe the characterization of other mutants recovered from the hydroxyurea resistance screen and how they implicate catalase and autophagy components in PCD. Although the vast majority of the hydroxyurea-resistant mutants were catalase deficient, we identified a single resistant mutant with normal catalase activity carrying a loss-of-function allele of the autophagy gene *ATG2*. We found that *atg2* and other autophagy component mutants showed reduced sensitivity to PCD induced by both hydroxyurea and avrRpm1. This dual loss of sensitivity, and the apparent specificity of the hydroxyurea resistance screen for catalase-related events, suggested that modulation of catalase activity might also play a role in avrRpm1-induced PCD. To test this hypothesis, we selected mutants with extremely low catalase activities but without lesions in *CATALASE2* (*CAT2*) and showed that *NCA1* is required for the activities of all three catalase isoforms in *Arabidopsis*. Both *cat2* and *nca1* mutants displayed loss of both avrRpm1 and hydroxyurea sensitivity. They also accumulated the selective autophagy target NBR1 and ubiquitinated proteins on avrRpm1 challenge, indicating that catalase activity is required to promote autophagy-dependent PCD.

RESULTS

Autophagy Is Required for Cell Death Induction by avrRpm1 and Hydroxyurea

We previously recovered 17 independent *CAT2* loss-of-function alleles in a screen for resistance to hydroxyurea-induced cell death

(Juul et al., 2010). To identify cell death signaling components acting downstream or independently of catalase, we screened for resistant mutants with normal catalase activity by quantifying the catalase activity levels of all isolated mutants. A single such mutant was found, and SHOREmap (Schneeberger et al., 2009) was used to identify a candidate premature stop mutation at amino acid 626 in the autophagy *ATG2* (*AT3G19190*) gene (see Supplemental Table 1 online). We designated this mutant *atg2-3*. Confirming correct identification of the causal mutation, the T-DNA line *atg2-1* (Yoshimoto et al., 2009, SALK_076727) was also resistant to hydroxyurea (Figure 1). In addition, *atg4a atg4b*, *atg5*, and *atg7* mutants displayed hydroxyurea resistance (Figure 1), showing that the resistance was not a specific property of the *atg2* mutants but rather depended on autophagy deficiency in general. By contrast, ENHANCED DISEASE SUSCEPTIBILITY1 and NON-RACE-SPECIFIC DISEASE RESISTANCE1, which are immune regulators acting downstream of R proteins, were not required for hydroxyurea sensitivity (Figure 1), indicating that the hydroxyurea signal acts independently or downstream of these signaling hubs.

NCA1 Is Required for Catalase Activity

The *atg5* and *atg7* mutants were previously reported to show attenuated RPM1-dependent PCD in response to avrRpm1 challenge (Hofius et al., 2009). Since the hydroxyurea resistance screen appeared highly selective for catalase-related events, the reduced hydroxyurea/avrRpm1 sensitivity of the autophagy mutants suggested that abnormal regulation of catalase activity might also interfere with avrRpm1 induced PCD. To test this hypothesis, we screened our collection of hydroxyurea resistant mutants for potential regulators of catalase activity. By sequencing the catalase genes of all mutants with reduced catalase activity, we identified two putative catalase regulator mutants with intact catalase genes but extremely low catalase activities, which we designated *nca1-1* and *nca1-2*.

In *Arabidopsis*, CAT2 activity is required for dissipation of photorespiration-derived H_2O_2, and the apparent growth retardation of *cat2* mutants is alleviated at high CO_2 concentrations as a result

Figure 1. Hydroxyurea Resistance of Autophagy and Immunity Mutants.

Seedlings germinated in the presence of 3 mM hydroxyurea. Unfolded green cotyledons indicate resistance to cell death induced by hydroxyurea. Ws, Wassilewskija.

[See online article for color version of this figure.]

of repression of photorespiration (Queval et al., 2007). Similarly to *cat2* mutants, the *nca1* mutants were resistant to hydroxyurea (Figure 2A) and showed reduced growth at ambient CO_2 levels (Figure 2B), which could be rescued by increasing the CO_2 concentration (Figure 2C). This classified the *nca1* alleles as photorespiratory mutants and suggested that their growth retardation phenotype could be explained by catalase deficiency.

The *nca1* mutants showed catalase activities below 5% of wild-type levels (Figure 2D). However, catalase transcript levels were similar to wild-type levels (Figure 2E), particularly for *CAT2*, which contributes the majority of catalase activity in green leaves. The amount of catalase protein was markedly decreased in both *nca1* mutants (Figure 2F) and the enzymatic activity of all three catalase isoforms was clearly decreased (Figure 2G), indicating that *NCA1* is required for the activity of all *Arabidopsis* catalases and acts mainly at the posttranscriptional level.

Using SHOREmap (Schneeberger et al., 2009), we identified an amino acid change at position 298 in AT3G54360 as a candidate causal mutation in *nca1-1* (Figure 2H; see Supplemental Table 2 online). The *nca1-2* allele contained a splice site–disrupting mutation in *AT3G54360* (Figure 2H). Furthermore, introduction of the *AT3G54360* gene into the *nca1-1* mutant background rescued the mutant phenotype (see Supplemental Figure 1 online). We conclude that *NCA1* is identical to *AT3G54360*.

The *NCA1* gene product contains a Really Interesting New Gene domain (cd00162), and its function has so far not been described. To get an indication whether the requirement of NCA1 for catalase activity is specific to *Arabidopsis* or more widely conserved, we searched for closely related genes in other plant species by querying the Phytozome plant gene family database (Goodstein et al., 2012). NCA1 is a member of an uncharacterized protein family (family 23249884), with one or two copies per plant genome in land plants (see Supplemental Figure 2 and Supplemental Data Set 1 online). Sequence conservation within the family is high, with 46% amino acid identity between NCA1 homologs from *Arabidopsis* and from the moss *Physcomitrella patens* (see Supplemental Table 3 online). Validating extensive evolutionary conservation of *NCA1* gene function, the *P. patens NCA1* cDNA complemented the *Arabidopsis nca1-1* mutant phenotype (see Supplemental Figures 1A and 1B online).

The *nca1* and *cat2* Mutants Display Similar Morphological Alterations, Oxidative Stress Responses, and Proteome Compositions

Because of the dramatic drop in catalase activity seen in the *nca1* mutants, we hypothesized that NCA1 might directly interact with catalase. Using NCA1 and CAT2 fusion protein constructs that complemented the respective mutant phenotypes, we found that CAT2, as expected, localized to punctate structures that most likely represent peroxisomes. NCA1, by contrast, localized to the cytosol and nucleus, making a direct interaction with CAT2 unlikely (Figure 3A). Since plant catalases localize to peroxisomes and their import depends on C-terminal peroxisomal targeting signals (Mullen et al., 1997), a second possibility was that NCA1 could influence peroxisomal integrity and thereby reduce catalase activity. However, we detected signals from the peroxisomal marker PTS1-GFP (for green fluorescent protein; Mano et al., 1999, 2002) in the *nca1-1*
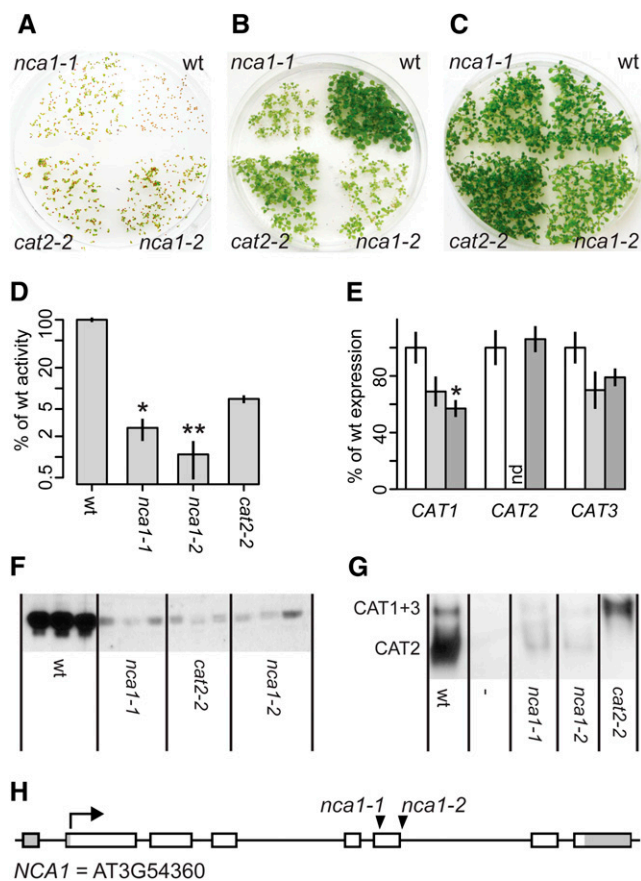

Figure 2. Characterization of the *nca1* Mutant Phenotype.

(A) to **(C)** Wild-type (wt), *nca1*, and *cat2* seedlings grown on one-half-strength MS supplemented with 3 mM hydroxyurea **(A)**, one-half-strength MS at ambient CO_2 level **(B)**, and one-half-strength MS at high CO_2 level **(C)**.

(D) to **(G)** Material from 12-d-old seedlings. Student's *t* test (two means) or one-way analysis of variance (ANOVA) and Dunnett's multiple comparison test was used for P value calculations.

(D) Comparison of catalase activity levels. All mutants differed significantly from the wild type (P < 0.0001). Both *nca1* mutants differed significantly from *cat2-2* (*P < 0.05 and **P < 0.01).

(E) Comparison of catalase transcript levels. White, Col-0 wild type; light gray, *cat2-2*; dark gray, *nca1-1*. nd, not detected. Only *CAT1* expression in the *nca1* background was significantly different from the wild type (*P < 0.05). Error bars indicate SE.

(F) Comparison of catalase protein levels as determined by immunoblotting. Three biological replicates are shown for each genotype.

(G) Zymogram showing activities of the different catalase isoforms. Three biological replicates were used, and a representative gel is shown.

(H) *NCA1* gene structure. Exons are shown as boxes. Untranslated regions are shown in gray. Mutations are indicated by triangles. See also Supplemental Figures 1 and 2 and Supplemental Tables 2 and 3 online. [See online article for color version of this figure.]

mutant background that appeared similar to those in the wild type, indicating that peroxisomes remained functional, at least with respect to PTS1-guided protein import (Figure 3A).

Since these localization experiments failed to identify an intimate2 association between catalase and NCA1, beyond the
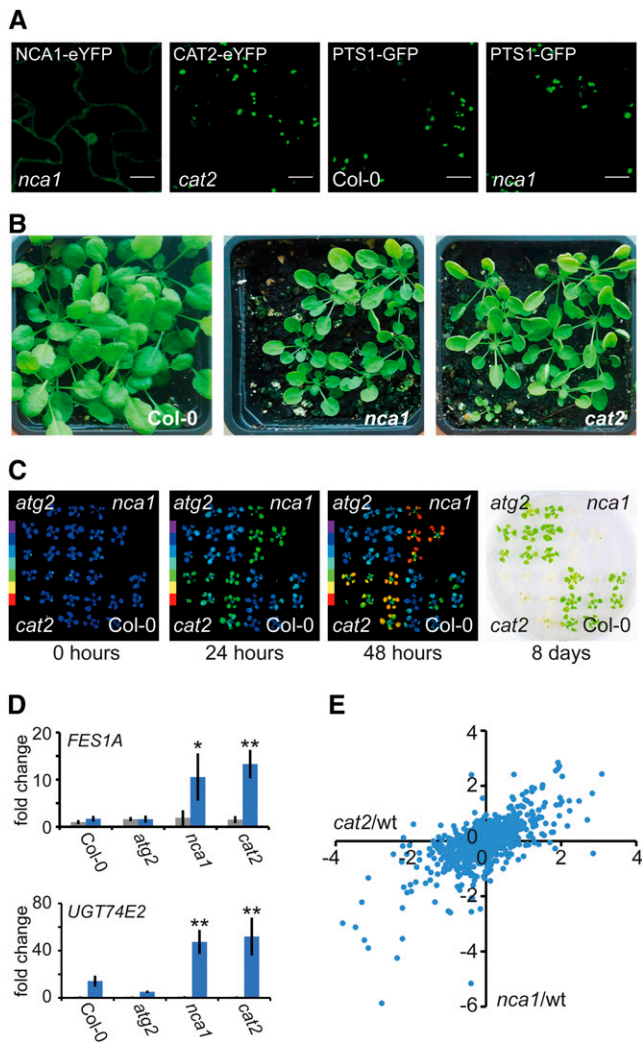
Figure 3. NCA1 and CAT2 Protein Localization and Mutant Phenotypes.

(A) Localization of the fusion proteins indicated in the top left corner in the genetic backgrounds shown in the bottom left corner. The NCA1-eYFP and CAT2-eYFP fusion proteins were driven by their native promoters, and PTS1-GFP was expressed from the cauliflower mosaic virus *35S* promoter. Bars = 10 μm.

(B) Four-week-old plants grown in short days on soil.

(C) Response to photorespiration-promoting growth conditions. The three leftmost panels show maximum quantum efficiency of photosystem II (*Fv/Fm*) on a heat map scale where red represents the lowest values. The experiment was performed in six replicates, and a representative plate is shown.

(D) Expression of oxidative stress marker genes. Fold changes with respect to the untreated Col-0 sample are shown. Gray bars indicate expression prior to photorespiratory stress treatment. Blue bars show expression after 24 h of treatment. Three replicates were used, and error bars indicate SE. Two-way ANOVA and Dunnett's multiple comparison test were used for calculating P values indicating the probability that an expression value was identical to the Col-0 value at the given time point ($*P < 0.05$ and $**P < 0.01$).

(E) Log_2 fold changes in protein abundances as determined by iTRAQ proteomics are plotted. Fold change values are based on three biological and four technical replicates. All quantified proteins were included in the plot. wt, wild type.

strongly reduced catalase activity in the *nca1* mutants, we performed a more detailed phenotypic analysis of the *nca1* and *cat2* mutants to evaluate their level of similarity. When grown on soil in short days, the *nca1* and *cat2* mutants were morphologically very similar, both displaying hyponastic leaves and reduced growth compared with the wild type (Figure 3B). Since both mutants were catalase deficient, we compared their oxidative stress responses. We imposed oxidative stress using a bioassay in which photorespiration-dependent H_2O_2 accumulation is induced by restricted gas exchange and simultaneous exposure to constant light conditions in Petri dishes. In contrast with the wild type and *atg2*, both *nca1* and *cat2* displayed decreased maximum quantum efficiency of photosystem II (*Fv/Fm*) within 24 h and died after 8 d of treatment (Figure 3C). Consistent with this aggravated response, both *nca1* and *cat2* displayed a stronger induction of expression of the oxidative stress marker genes *FACTOR EXCHANGE FOR SSA1 PROTEIN1A* and *URIDINE DIPHOSPHATE GLYCOSYLTRANSFERASE 74E2* (Tognetti et al., 2010; Inzé et al., 2012) than did the wild type and *atg2* after 24 h of oxidative stress treatment (Figure 3D). The hypersensitivity to oxidative stress for both mutants is consistent with the rescue of their growth retardation phenotype by increased CO_2 levels, which suppress photorespiration (Figures 2B and 2C).

These strong similarities indicated that the morphological aberrations and oxidative stress responses of the *nca1* mutant could be explained by catalase deficiency. However, it was still possible that NCA1 could affect the abundance of other proteins in addition to catalase, which would result in protein level perturbations exclusive to the *nca1* mutant. To investigate this possibility, we compared the proteomes of short-day-grown wild-type, *nca1*, and *cat2* plants using isobaric tags for relative and absolute quantitation (iTRAQ) labeling. We detected and quantified a total of 933 proteins (see Supplemental Data Set 2 online). For comparison with the catalase immunoblots and activity measurements (Figures 2D, 2F, and 2G), we first looked more closely at the peptides unique to the three catalase isoforms. We identified no unique CAT1 peptides. CAT2 peptides were not detected in the *cat2* mutant and were found at ~6% of wild-type levels in *nca1* mutants, whereas CAT3 peptides were detected at reduced levels in both *nca1* and *cat2* mutants (see Supplemental Tables 4 and 5 online). The CAT2 peptide data matches the in-gel CAT2 activity data, showing reduced activity in *nca1* and no detectable activity in *cat2* (Figure 2G). The reduction in CAT3 peptide abundance matches the reduced activity seen in *nca1*, whereas *cat2* appeared to have no reduction in the catalase activity derived from CAT1 and CAT3 (Figure 2G). This apparent discrepancy could be explained either by a large contribution from CAT1, which we were unable to quantify using our proteomics approach or by different levels of activity of the residual CAT3 protein in the two mutants. To evaluate the overall similarity of the *nca1* and *cat2* proteomes, we then compared their global changes in protein abundance with respect to the wild-type control. The fold changes in the two mutants were highly correlated (Figure 3E) with a Pearson correlation coefficient of 0.66. Inspecting the proteins displaying the highest fold changes for each mutant, we found that ~50% of the top 80 regulated proteins overlapped between *nca1* and *cat2*, further
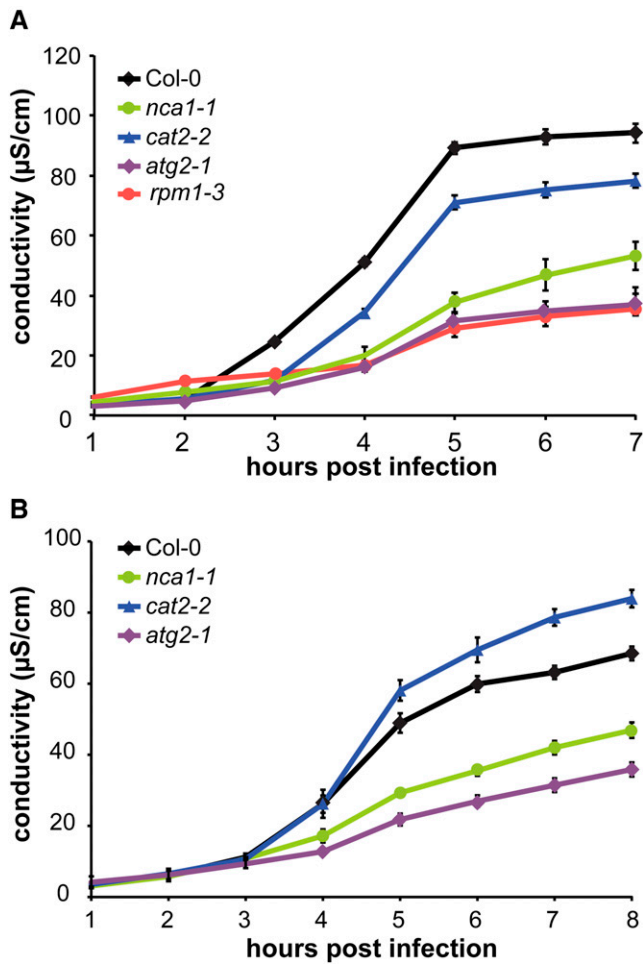
Figure 4. Suppression of *Pst* DC3000 *avrRpm1*–Mediated Cell Death in Catalase- and Autophagy-Deficient Mutants.

Ion leakage measurements of the wild type (Col-0), *rpm1-3*, *cat2-2*, *nca1-1*, and *atg2-1* after inoculation with a (OD_{600} = 0.2) culture of avirulent *Pst* DC3000 expressing *avrRpm1*.
(A) Four-week-old short-day-grown plants.
(B) Four-week-old short-day-grown plants shifted to long days 3 d prior to infection. Mean and SE were calculated from four leaf discs per treatment, with four replicates per experiment.

underlining the similarity of the two mutant proteomes (see Supplemental Data Set 3 online).

Catalase Activity Is Required for Cell Death Induction by *avrRpm1* and Hydroxyurea

Based on morphology, oxidative stress response, and proteome characteristics, the *nca1* mutant phenotype could be explained by catalase deficiency. NCA1 was thus specifically required for the activity of all catalase isoforms in *Arabidopsis*. These properties make the *nca1* mutant well suited for testing our hypothesis that catalase activity is required for sensitivity to both hydroxyurea and avrRpm1-induced cell death. We therefore quantified the avrRpm1 cell death response in short-day-grown

plants and found that both *cat2* and *nca1* mutants showed an attenuated response. The *nca1* mutant displayed a stronger reduction in the PCD response, consistent with its lower catalase activity levels (Figure 4A). Overexpression of *NCA1* from the cauliflower mosaic virus *35S* promoter in the *nca1* mutant background partially rescued the PCD response, but it did not result in cell death levels higher than those seen in the wild type (see Supplemental Figure 1 online). Restriction of catalase activities through transcriptional repression of *NCA1* does therefore not appear to play a role during avrRpm1-induced PCD. We also found a strongly attenuated cell death response for the *atg2* mutant (Figure 4), confirming that it had lost both its sensitivity to hydroxyurea and its ability to induce cell death in response to avrRpm1.

Although the attenuated avrRpm1 cell death response of the catalase-deficient mutants agrees well with their identification in our screen for resistance to hydroxyurea-induced cell death, it is controversial because the opposite phenotype, exaggerated cell death responses, has previously been reported for the *cat2* mutant (Queval et al., 2007; Chaouch et al., 2010). According to these studies, the *cat2* exaggerated cell death phenotype is daylength dependent. Since the plants used for our cell death assay were grown in short days, but the *cat2* cell death phenotype manifests itself in longs days (Queval et al., 2007; Chaouch et al., 2010), we investigated whether a difference in light conditions could explain the discrepancy. Indeed, shifting the plants to long days 3 d prior to avrRpm1 challenge resulted in an aggravated response in the *cat2* mutant, while cell death remained suppressed in *nca1* (Figure 4B).

Cell Death and Bacterial Resistance Are Uncoupled in *nca1*, *cat2*, and *atg2* Mutants

Since the catalase- and autophagy-deficient mutants showed an attenuated cell death response, plant immunity to bacterial infection could also be compromised. However, measuring
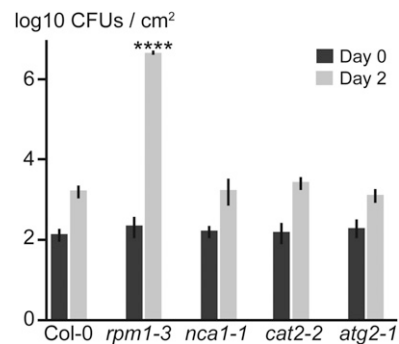

Figure 5. *Pst* DC3000 *avrRpm1* Resistance Characteristics of Catalase and Autophagy-Deficient Mutants.

Growth of *Pst* DC3000 *avrRpm1* in leaves of 5-week-old plants at 0 and 2 d after infiltration with 1×10^5 CFU mL^{-1}. Log-transformed values are means ± SD (n = 3). Two-way ANOVA and Dunnett's multiple comparison test were used for calculating P values indicating the probability that a CFU value was identical to the Col-0 value at the given time point (****P < 0.0001).
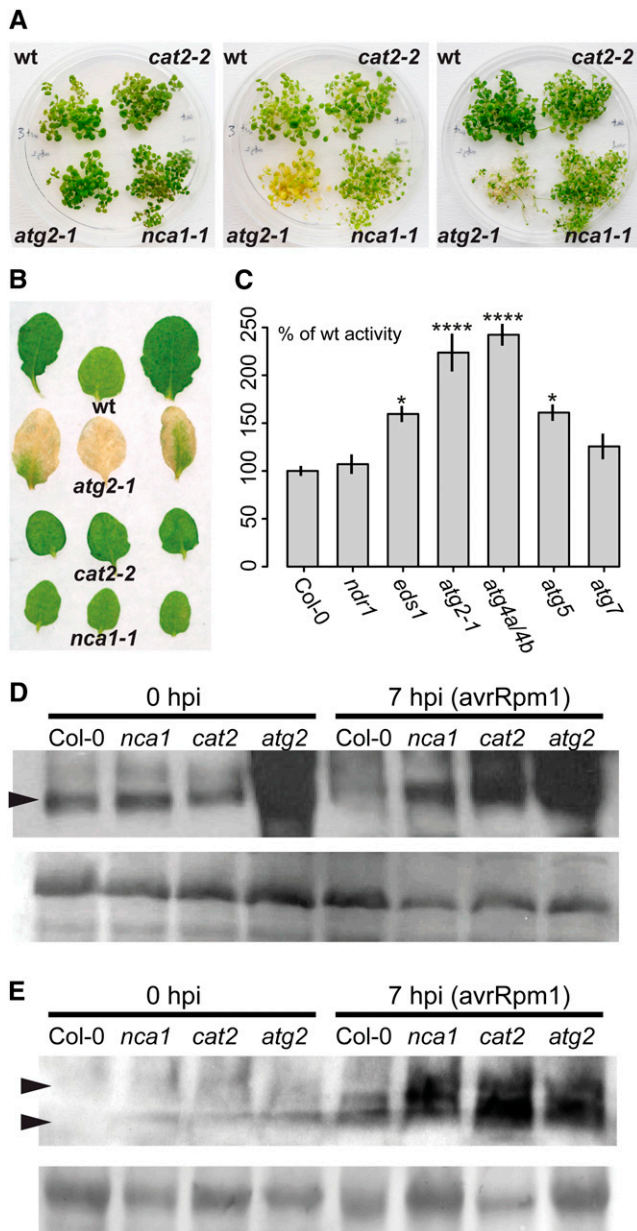
A

B

C

D

E

Figure 6. Catalase and Autophagy Interactions.

(A) Prolonged darkness assay. Left panel, prior to dark treatment; middle panel, after 10 d in darkness; right panel, after 10 d in darkness and 10 d of recovery in light. wt, the wild type.

(B) Detached leaves incubated on moist filter paper for 3 d.

(C) Catalase activities of immune effector and autophagy mutants. Error bars show sᴇ, and three replicates were used. P values indicating the probabilities that the activity levels were identical to the wild-type level were calculated using a one-way ANOVA followed by Dunnett's test for multiple comparisons. (*P < 0.05 and ****P < 0.0001).

(D) NBR1 immunoblot on extracts from plants prior to and 7 h after inoculation (hpi) with *Pst* DC3000 *avrRpm1*. Arrowhead indicates the position of the NBR1 band. The bottom panel shows the Ponceau-stained membrane.

(E) Ubiquitin immunoblot on extracts from plants prior to and 7 h after inoculation with *Pst* DC3000 *avrRpm1*. The top panel shows ubiquitinylated

bacterial growth after infiltration showed that this was not the case. As expected, RPM1 was required for immunity, but the *nca1*, *cat2*, and *atg2* mutants did not display increased bacterial growth compared with the wild type (Figure 5). Reminiscent of the *Arabidopsis* type I metacaspase mutant *mc1* (Coll et al., 2010), the *nca1*, *cat2,* and *atg2* mutants therefore uncouple *Pto*DC3000 (*avrRpm1*)–induced cell death from induced resistance.

Catalase Acts Upstream of Autophagy in the avrRpm1 Response

To determine the relative positions of catalase and autophagy within the PCD signaling network, we first investigated the autophagy properties of catalase mutants, and vice versa, to confirm that PCD was suppressed due to defects in distinct processes in the two groups of mutants. Autophagy is induced during starvation and senescence, and lack of autophagic components leads to hypersensitivity to nutrient limitation (Doelling et al., 2002). Leaf detachment induces senescence (Weaver et al., 1998), whereas exposure to prolonged darkness leads to carbon starvation (Thompson et al., 2005). In contrast with the *atg2-1* mutant, *nca1-1* and *cat2-2* did not show exaggerated senescence in response to leaf detachment or prolonged darkness (Figures 6A and 6B). This argues that autophagy starvation and senescence responses are not compromised in the *nca1* and *cat2* mutants and that the reduced cell death response on avrRpm1 challenge is not caused by a general lack of autophagy competence in these mutants. Conversely, the *atg* mutants all showed catalase activities at or above wild-type levels (Figure 6C), allowing us to rule out that the *atg* mutants displayed reduced hydroxyurea and avrRpm1 sensitivity as a result of catalase deficiency. Autophagy competence and catalase activity therefore both appear to be required for full sensitivity to hydroxyurea and avrRpm1-induced cell death.

To investigate if catalase acts upstream of autophagy in the avrRpm1 response, we examined the immunity-induced autophagy response of the catalase-deficient mutants. *Arabidopsis* NBR1 is a target of selective autophagy that accumulates in autophagy-deficient mutants (Svenning et al., 2011). Prior to avrRpm1 challenge, the NBR1 levels were similar in the wild type, *nca1*, and *cat2* mutants, whereas the *atg2* mutant showed strong NBR1 accumulation (Figure 6D). This reflects that even in the absence of starvation or senescence challenge, a basal level of autophagy is needed to prevent NBR1 accumulation. This basal activity is absent in the *atg2* mutant but still present in other genotypes, confirming the autophagy competence of the *nca1* and *cat2* mutants. After avrRpm1 challenge, the NBR1 level remained low in protein extracts from wild-type plants 7 h after infection (Figure 6D). In marked contrast, NBR1 had accumulated to high levels in protein extracts from *nca1*, *cat2*, and *atg2* mutants (Figure 6D). To confirm the aberrant immunity-induced autophagy phenotype of the catalase-deficient mutants, we assayed the abundance of ubiquitinated proteins, which accumulate in

proteins. The top and bottom arrowheads indicate sizes of 55 and 60 kD, respectively. The bottom panel shows the Ponceau-stained membrane. [See online article for color version of this figure.]

autophagy-deficient mutants under heat stress (Zhou et al., 2013). In contrast with the wild type, we found that *nca1*, *cat2*, and *atg2* all displayed accumulation of ubiquitinated proteins 7 h after infection (Figure 6E). The differential accumulation of both NBR1 and ubiquitinated proteins shows that the autophagic degradation triggered by RPM1 is severely inhibited in the catalase-deficient mutants and indicates that catalase acts upstream of immunity-triggered autophagy during promotion of PCD (Figure 7).

DISCUSSION

Autophagy: Promotion or Attenuation of PCD?

It was the identification of the autophagy *atg2-3* mutant in our screen for resistance to hydroxyurea-induced cell death combined with its reduced sensitivity to avrRpm1-elicited PCD that led us to suspect a similar dual loss of sensitivity for the catalase-deficient mutants recovered from the same screen. Other autophagy components are required for PCD downstream of R protein effector recognition (Hofius et al., 2009) and display hydroxyurea resistance (Figure 1). However, autophagy is also important for removal of cellular waste products, and autophagy deficiency leads to premature senescence accompanied by cell death (Yoshimoto et al., 2009). Interestingly, limiting the spread of pathogen-induced PCD appears to depend on autophagy too, suggesting a negative, rather than positive, role in PCD regulation (Liu et al., 2005; Patel and Dinesh-Kumar, 2008; Yoshimoto et al., 2009). The uncontrolled spread of HR PCD in autophagy

Figure 7. Tentative Model for Catalase Integration of PCD Signals.

In our screen for hydroxyurea resistance, the death of wild-type plants at germination coincides with ROS generation as a byproduct of β-oxidation of fatty acids during seed storage oil mobilization. These ROS activate catalase, which interacts directly with hydroxyurea to produce an autophagy-dependent PCD response. AvrRpm1 challenge causes a HR comprising an oxidative burst. The ROS produced activate catalase, which reacts with unknown compounds to generate an autophagy-dependent PCD response. Resistance to *Pst* DC3000 *avrRpm1* is induced independently of the PCD response mediated by catalase and autophagy proteins. Cell death inducers (red) and genetic components (blue) investigated in this study are highlighted.

mutants was observed only in older leaves of 7- to 8-week-old plants and not in younger tissues (Yoshimoto et al., 2009). It could thus reflect that a tissue already poised for senescence is pushed over the edge by a pathogen-induced HR. These observations suggest that different ages of the plant material used in the cell death assays offer a likely explanation for the apparent discrepancies in the reports on autophagy-dependent regulation of PCD.

Our identification of an autophagy component in a forward genetic screen for resistance to hydroxyurea-induced cell death and the strong suppression of avrRpm1-induced PCD seen in the *atg2* mutant, which also shows a stronger premature senescence phenotype than other autophagy mutants (Yoshimoto et al., 2009), emphasizes the role of autophagy in promotion of PCD.

Catalase Acts as Both an Antioxidative Enzyme and a PCD Effector

In contrast with autophagy, catalase activity has so far exclusively been associated with attenuation of cell death and not with its promotion. Since ROS can induce PCD and damage cellular proteins and membranes, loss of antioxidative enzyme activity, including that of catalase, could be detrimental to the plant and result in aggravated cell death responses. There is a large body of evidence to support this view. In *Arabidopsis*, this includes observations that *cat2* mutants display a photoperiod-conditional cell death phenotype, which is dependent on salicylic acid production and manifests itself under long-day conditions (Queval et al., 2007; Chaouch et al., 2010). These results indicated that catalase deficiency induces an HR-like PCD under growth conditions favoring accumulation of peroxisomal H_2O_2, which led the authors to suggest that suppression of catalase activity may play a role in establishing the oxidative burst and executing PCD during pathogen defense (Chaouch et al., 2010). Light-dependent lesions were also observed in earlier studies using tobacco (*Nicotiana tabacum*) catalase antisense lines. In addition, aggravated cell death responses and increased resistance to pathogens was observed (Chamnongpol et al., 1998; Mittler et al., 1999; Dat et al., 2003).

Our results now reveal that catalase has an additional, and opposite, role in promoting PCD. This conclusion is supported both by the identification of mutant alleles of catalase and *NCA1* in our genetic screen for resistance to hydroxyurea-induced cell death and by the suppression of avrRpm1-induced cell death observed for these mutants. The PCD-promoting role of catalase has likely been masked in previous studies by the use of high-stress light conditions. As we have shown here, altering the daylength during plant growth is sufficient to change the nature of the *cat2* cell death response (Figure 4).

Catalase requires activation by one molecule of H_2O_2 to enter its activated state, where it can either react with a second molecule of H_2O_2 or with other substrates (Chance, 1947). We suggest that during a HR, catalase is activated by high levels of H_2O_2 and reacts with an unknown substrate to generate a PCD-activating signal (Figure 7). If catalase levels are insufficient, the PCD signal is suppressed. According to this working model, the *cat2* mutant, which retains some residual catalase activity, would still be able to induce PCD in response to pathogen challenge, and the response would be compounded by combination
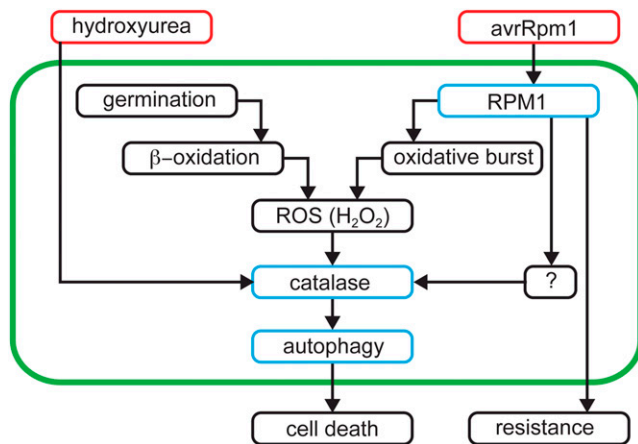
with severe oxidative stress (Figure 4). By contrast, the very low residual catalase activity in the *nca1* mutant would be insufficient to cause immunity-induced PCD even in combination with high oxidative stress levels (Figure 4B). The residual catalase activity in the *cat2* mutant is derived from *CAT1* and/or *CAT3*, which reside in a tandem repeat on *Arabidopsis* chromosome 1. Based on available microarray data, *CAT3* expression appears to overlap with that of *CAT2* in leaves and seeds, whereas *CAT1* shows weaker expression in these tissues but is strongly expressed in pollen (Schmid et al., 2005; Winter et al., 2007). One or both of these other catalase isoforms likely also contribute to the catalase-dependent PCD response. This conclusion is based on the overall similarity of the *nca1* and *cat2* phenotypes combined with the clear differences in catalase activities in the two mutants. However, we cannot rule out that the *nca1* mutant displays more strongly reduced avrRpm1 sensitivity than *cat2* because of the regulation of other unknown targets in addition to the catalases.

Is Catalase a Direct Molecular Link between ROS and PCD Signaling?

The similarities between the PCD responses induced by hydroxyurea and avrRpm1 are striking. First, *NCA1*, *CAT2*, and autophagy genes make up a common set of genetic components required for the PCD responses to both inducers. Second, as catalase interacts directly with hydroxyurea (Juul et al., 2010), it likely acts upstream of autophagy components in hydroxyurea-induced PCD, as it does in PCD induced by avrRpm1 (Figures 6D to 6F). Third, the PCD responses induced by both hydroxyurea and avrRpm1 are associated with generation of ROS. On avrRpm1 challenge, ROS are produced during the HR oxidative burst (Doke, 1983). In the hydroxyurea resistance screen, the death of the wild-type plants at ~2 d after germination coincides with ROS production during the respiratory burst accompanying the β-oxidation of fatty acids typical for storage oil mobilization in oilseed plants (Graham, 2008). After germination, *Arabidopsis* plants are much less sensitive to hydroxyurea, as evidenced by their survival on medium containing 25 mM hydroxyurea in the hydroxyurea uptake assay described by Juul et al. (2010).

Although hydroxyurea and catalase interact directly, and hydroxyurea acts as a competitive inhibitor of H_2O_2 decomposition (Juul et al., 2010), hydroxyurea does not induce PCD by overloading the system with ROS through catalase inhibition, since loss-of-function catalase mutations are resistant to hydroxyurea. The most likely explanation is instead that the combination of catalase activation by H_2O_2 and the presence of hydroxyurea generate a signal, which activates autophagy-dependent PCD. Considering the similarities between PCD induced by hydroxyurea and avrRpm1, the catalase-dependent signal activating autophagy-dependent PCD upon avrRpm1 challenge could well be similar in nature to the signal resulting from the interaction between catalase and hydroxyurea. Validation of this working model (Figure 7) will require identification of the putative signaling compounds, which is challenging because of the radical chemistry involved. However, the association of hydroxyurea, catalase, and autophagy with PCD paves the way for further advances in our understanding of the causal relationship between the oxidative burst and PCD in plant defense.

METHODS

Plant Materials and Growth Conditions

The hydroxyurea resistance screen was performed as described (Juul et al., 2010), screening for germination at a concentration of 3 mM hydroxyurea. Plants for catalase assays, transcript quantification, and immunoblots were grown on plates as previously described (Juul et al., 2010) and harvested 12 d after germination. Plants for ion leakage and detached leaf assays were grown on soil as described (Hofius et al., 2009). Long-day growth conditions were equivalent to the short-day conditions except for the 16-h daylength. Plants for CO_2 rescue were grown in growth chambers at 22°C, 16/8-h light/dark cycles, and 150 μmol m^{-2}s^{-1} photosynthetic photon flux at either 0.04% (ambient) or 0.4% (elevated) CO_2 levels on one-half-strength Murashige and Skoog (MS) medium (Duchefa) solidified with 0.9% agar. For the prolonged darkness assay, plants were grown as described (Juul et al., 2010) for 12 d, incubated for 10 d in darkness, and finally moved back to normal light conditions for 10 d.

Induction of Oxidative Stress and *Fv/Fm* Quantification

We used a bioassay in which photorespiration is induced by restricting gas exchange within Petri dishes. For the photorespiration-promoting conditions, plants were grown on one-half-strength MS agar medium for 2.5 weeks. Then, the plates were transferred to a continuous light regime after replacing the surgical tape (Micropore; 3M) that sealed the plates by two layers of Parafilm M (Alcan) to restrict gas exchange. The maximum efficiency of the photosystem II photochemistry (*Fv/Fm*) was determined using a PAM-2000 chlorophyll fluorometer.

Analysis of Catalase Activities and Transcript and Protein Abundances

Catalase activity was quantified as described (Beers and Sizer, 1952). For catalase transcript quantification, RNA was extracted from 12-d-old seedlings using the Nucleospin RNA plant kit (Macherey Nagel). Following DNase I treatment, cDNA was prepared using the RevertAid first-strand cDNA synthesis kit (Fermentas). As internal controls, the transcript levels of two previously characterized control genes At5g25760 and At1g13320 (Czechowski et al., 2005) were quantified. Primers are listed in Supplemental Table 6 online. For quantification of the oxidative stress marker genes *FACTOR EXCHANGE FOR SSA1 PROTEIN1A* (At3g09350) and *URIDINE DIPHOSPHATE GLYCOSYLTRANSFERASE74E2* (At1g05680), RNA isolation, cDNA synthesis, and quantitative RT-PCR analyses were performed as described (Tognetti et al., 2010). Immunoblots and zymogram analyses were performed as previously described (McClung, 1997; Vandenabeele et al., 2004). For NBR1 and ubiquitin, protein was extracted in urea buffer from plants syringe-infiltrated with 2×10^8 colony-forming units (CFU) mL^{-1} of avirulent *Pst avrRpm1* and detected with anti-NBR1 antibody as described (Svenning et al., 2011) or with anti-ubiquitin antibody (Zhou et al., 2013). Statistical analyses were performed using GraphPad Prism 6.0.

SHOREmap Causal Mutant Identification

The *nca1-1* and *atg2-3* causal mutations were identified using the SHOREmap approach (Schneeberger et al., 2009). Landsberg *erecta* was used as the mapping parent, and pools of 499 (*nca1-1*) and 323 (*atg2-2*) F2 plants were sequenced to ~7× genome coverage.

Mutant Complementation and Protein Localization

The *NCA1* promoter was amplified from Columbia-0 (Col-0) genomic DNA and cloned into a pGreen0029 (Hellens et al., 2000) vector carrying

a Gateway (GW) cassette using restriction sites *Kpn*I and *Hind*III followed by enhanced yellow fluorescent protein (eYFP; Shaner et al., 2004) amplification and cloning into the pGreen0029-pNCA1-GW plasmid using the *Hind*III site to construct a pGreen0029-pNCA1-eYFP-GW (pMC-00637) plasmid. The same strategy was used for cloning the CAT2 promoter to construct the pGreen0029-pCAT2-eYFP-GW (PMC-00642) plasmid. NCA1 genomic DNA excluding promoter was amplified from Col-0 genomic DNA and recombined into the pMC-00637 plasmid to create the pGreen0029-pNCA1-eYFP-NCA1 (pMC-00638, *pNCA1:NCA1*) in-frame fusion expression construct. *NCA1* cDNA was amplified from the U13379 clone, obtained from the ABRC, and then recombined into a pEarleyGate104 vector (Earley et al., 2006) to create the pEarleyGate-35S-YFP-NCA1 (pMC-00570, *35S: NCA1*) construct. *Physcomitrella patens NCA1* cDNA was amplified from RNA extracted as described (Cove et al., 2009) and recombined into pEarleyGate104 to create the pEarleyGate-35S-YFP-PpNCA1 (pMC-00588, *35S:PpNCA1*) construct. *CAT2* cDNA was amplified from RNA extracted as described (Cove et al., 2009) and recombined into PMC-00642 to create the pGreen0029-pCAT2-eYFP-CAT2 (PMC-00647) expression construct. Live tissue was observed under a Zeiss 510 Meta confocal microscope to image fusion protein localization.

Conductivity Measurements and Resistance Assays

Bacterial ion leakage assays following syringe infiltration of avirulent *Pst avrRpm1* were performed with 2×10^8 CFU mL^{-1}, and bacterial growth was determined at days 0 and 2 after infection with 1×10^5 CFU mL^{-1} as described (Mackey et al., 2003). The *rpm1-3* null mutant (Grant et al., 1995) was used as control.

iTRAQ Proteomics

Tissue was collected from wild-type, *cat2*, and *nca1* plants grown for 3.5 weeks in short days. Protein was extracted in PBS buffer, ultracentrifuged, phenol extracted, precipitated, and then redissolved. Next, disulfide bonds were reduced and protein was alkylated prior to trypsin digestion. The resulting peptides were purified and dried. After redissolving, peptides were quantified and labeled using 4-plex iTRAQ reagents (Applied Biosystems) followed by HILIC fractionation on a microHPLC system. The labeled peptides were then subjected to liquid chromatography–tandem mass spectrometry analysis using a LTQ-Orbitrap XL mass spectrometer (Thermo Fisher Scientific) for data collection. Finally, the raw data were deconvoluted and converted into peak lists by ProteomeDiscoverer software version 1.2 (Thermo Scientific). The peak lists were then used for searches against the *Arabidopsis thaliana* proteome using Mascot version 2.3. See Supplemental Methods 1 online for full details.

Accession Numbers

Sequence data from this article can be found in the Arabidopsis Genome Initiative database under the accession numbers listed in Supplemental Table 7 online.

Supplemental Data

The following materials are available in the online version of this article.

   Supplemental Figure 1. Complementation of the *nca1* Mutant Phenotype.

   Supplemental Figure 2. *NCA1* Phylogeny.

   Supplemental Table 1. SHOREmap Output for the *atg2-3* Mutant.

   Supplemental Table 2. SHOREmap Output for the *nca1-1* Mutant.

   Supplemental Table 3. Comparison of NCA1 Protein Sequences across Species.

   Supplemental Table 4. Unique Catalase Peptides.

   Supplemental Table 5. iTRAQ Proteomics Experiment Setup.

   Supplemental Table 6. Oligonucleotide Sequences.

   Supplemental Table 7. Accession Numbers.

   Supplemental Data Set 1. NCA1 Protein Alignment.

   Supplemental Data Set 2. iTRAQ Proteomics Results.

   Supplemental Data Set 3. Top Up- and Downregulated Proteins for the *nca1* and *cat2* Mutants.

   Supplemental Methods 1. Phylogenetic Analysis and iTRAQ Methods.

AUTHOR CONTRIBUTIONS

T.H. made all *NCA1* constructs and produced and characterized all transgenic plant lines. S.G. and A.A. measured catalase activities and quantified catalase transcript levels. T.J., A.M., and S.U.A. did hydroxyurea resistance screening and produced mapping populations. T.J. characterized hydroxyurea resistance of *atg* mutants and conducted the prolonged darkness assay. A.A. performed the CO_2 rescue experiment and cloned *P. patens NCA1*. K.L.N. did the Illumina sequencing. J.-E.J. contributed with ideas and discussions. K.V.D.K. and F.V.B. contributed with phenotyping, catalase protein gel blots, in-gel activity assays, and discussions. M.P., D.H., and S.B. contributed with ion leakage measurements, resistance and leaf detachment assays, discussions, and NBR1 and ubiquitin protein gel blots. S.D., A.L., and P.R. carried out the proteomics study. S.U.A. designed the research, analyzed sequencing data, conducted the phylogenetic analysis, and wrote the article.

REFERENCES

Ausubel, F.M. (2005). Are innate immune signaling pathways in plants and animals conserved? Nat. Immunol. **6:** 973–979.

Beers, R.F., Jr., and Sizer, I.W. (1952). A spectrophotometric method for measuring the breakdown of hydrogen peroxide by catalase. J. Biol. Chem. **195:** 133–140.

Chamnongpol, S., Willekens, H., Moeder, W., Langebartels, C., Sandermann, H., Jr., Van Montagu, M., Inzé, D., and Van Camp, W. (1998). Defense activation and enhanced pathogen tolerance induced by H2O2 in transgenic tobacco. Proc. Natl. Acad. Sci. USA **95:** 5818–5823.

Chance, B. (1947). An intermediate compound in the catalase-hydrogen peroxide reaction. Acta Chem. Scand. **1:** 236–267.

Chaouch, S., Queval, G., Vanderauwera, S., Mhamdi, A., Vandorpe, M., Langlois-Meurinne, M., Van Breusegem, F., Saindrenan, P., and Noctor, G. (2010). Peroxisomal hydrogen peroxide is coupled to biotic defense responses by ISOCHORISMATE SYNTHASE1 in a daylength-related manner. Plant Physiol. **153:** 1692–1705.

Coll, N.S., Vercammen, D., Smidler, A., Clover, C., Van Breusegem, F., Dangl, J.L., and Epple, P. (2010). *Arabidopsis* type I metacaspases control cell death. Science **330:** 1393–1397.

Cove, D.J., Perroud, P.-F., Charron, A.J., McDaniel, S.F., Khandelwal, A., and Quatrano, R.S. (2009). Isolation of DNA, RNA, and protein from the moss *Physcomitrella patens* gametophytes. Cold Spring Harb Protoc **2009:** t5146.

Czechowski, T., Stitt, M., Altmann, T., Udvardi, M.K., and Scheible, W.-R. (2005). Genome-wide identification and testing of superior reference genes for transcript normalization in Arabidopsis. Plant Physiol. **139:** 5–17.

Dat, J.F., Pellinen, R., Beeckman, T., Van De Cotte, B., Langebartels, C., Kangasjärvi, J., Inzé, D., and Van Breusegem, F. (2003). Changes in hydrogen peroxide homeostasis trigger an active cell death process in tobacco. Plant J. **33:** 621–632.

Doelling, J.H., Walker, J.M., Friedman, E.M., Thompson, A.R., and Vierstra, R.D. (2002). The APG8/12-activating enzyme APG7 is required for proper nutrient recycling and senescence in *Arabidopsis thaliana*. J. Biol. Chem. **277:** 33105–33114.

Doke, N. (1983). Involvement of superoxide anion generation in the hypersensitive response of potato tuber tissues to infection with an incompatible race of *Phytophthora infestans* and to the hyphal wall components. Physiol. Plant Pathol. **23:** 345–357.

Earley, K.W., Haag, J.R., Pontes, O., Opper, K., Juehne, T., Song, K., and Pikaard, C.S. (2006). Gateway-compatible vectors for plant functional genomics and proteomics. Plant J. **45:** 616–629.

González-Lamothe, R., Tsitsigiannis, D.I., Ludwig, A.A., Panicot, M., Shirasu, K., and Jones, J.D.G. (2006). The U-box protein CMPG1 is required for efficient activation of defense mechanisms triggered by multiple resistance genes in tobacco and tomato. Plant Cell **18:** 1067–1083.

Goodstein, D.M., Shu, S., Howson, R., Neupane, R., Hayes, R.D., Fazo, J., Mitros, T., Dirks, W., Hellsten, U., Putnam, N., and Rokhsar, D.S. (2012). Phytozome: A comparative platform for green plant genomics. Nucleic Acids Res. **40** (Database issue)**:** D1178–D1186.

Graham, I.A. (2008). Seed storage oil mobilization. Annu. Rev. Plant Biol. **59:** 115–142.

Grant, M.R., Godiard, L., Straube, E., Ashfield, T., Lewald, J., Sattler, A., Innes, R.W., and Dangl, J.L. (1995). Structure of the Arabidopsis RPM1 gene enabling dual specificity disease resistance. Science **269:** 843–846.

Hellens, R.P., Edwards, E.A., Leyland, N.R., Bean, S., and Mullineaux, P.M. (2000). pGreen: A versatile and flexible binary Ti vector for Agrobacterium-mediated plant transformation. Plant Mol. Biol. **42:** 819–832.

Hofius, D., Munch, D., Bressendorff, S., Mundy, J., and Petersen, M. (2011). Role of autophagy in disease resistance and hypersensitive response-associated cell death. Cell Death Differ. **18:** 1257–1262.

Hofius, D., Schultz-Larsen, T., Joensen, J., Tsitsigiannis, D.I., Petersen, N.H.T., Mattsson, O., Jørgensen, L.B., Jones, J.D.G., Mundy, J., and Petersen, M. (2009). Autophagic components contribute to hypersensitive cell death in *Arabidopsis*. Cell **137:** 773–783.

Inzé, A., Vanderauwera, S., Hoeberichts, F.A., Vandorpe, M., Van Gaever, T., and Van Breusegem, F. (2012). A subcellular localization compendium of hydrogen peroxide-induced proteins. Plant Cell Environ. **35:** 308–320.

Jabs, T., Dietrich, R.A., and Dangl, J.L. (1996). Initiation of runaway cell death in an *Arabidopsis* mutant by extracellular superoxide. Science **273:** 1853–1856.

Jones, J.D.G., and Dangl, J.L. (2006). The plant immune system. Nature **444:** 323–329.

Juul, T., Malolepszy, A., Dybkaer, K., Kidmose, R., Rasmussen, J.T., Andersen, G.R., Johnsen, H.E., Jørgensen, J.-E., and Andersen, S.U. (2010). The in vivo toxicity of hydroxyurea depends on its direct target catalase. J. Biol. Chem. **285:** 21411–21415.

Lamb, C., and Dixon, R.A. (1997). The oxidative burst in plant disease resistance. Annu. Rev. Plant Physiol. Plant Mol. Biol. **48:** 251–275.

Liu, Y., Schiff, M., Czymmek, K., Tallóczy, Z., Levine, B., and Dinesh-Kumar, S.P. (2005). Autophagy regulates programmed cell death during the plant innate immune response. Cell **121:** 567–577.

Mackey, D., Belkhadir, Y., Alonso, J.M., Ecker, J.R., and Dangl, J.L. (2003). *Arabidopsis* RIN4 is a target of the type III virulence effector AvrRpt2 and modulates RPS2-mediated resistance. Cell **112:** 379–389.

Mano, S., Hayashi, M., and Nishimura, M. (1999). Light regulates alternative splicing of hydroxypyruvate reductase in pumpkin. Plant J. **17:** 309–320.

Mano, S., Nakamori, C., Hayashi, M., Kato, A., Kondo, M., and Nishimura, M. (2002). Distribution and characterization of peroxisomes in *Arabidopsis* by visualization with GFP: Dynamic morphology and actin-dependent movement. Plant Cell Physiol. **43:** 331–341.

McClung, C.R. (1997). Regulation of catalases in *Arabidopsis*. Free Radic. Biol. Med. **23:** 489–496.

Mittler, R., Herr, E.H., Orvar, B.L., van Camp, W., Willekens, H., Inzé, D., and Ellis, B.E. (1999). Transgenic tobacco plants with reduced capability to detoxify reactive oxygen intermediates are hyperresponsive to pathogen infection. Proc. Natl. Acad. Sci. USA **96:** 14165–14170.

Mizushima, N. (2007). Autophagy: Process and function. Genes Dev. **21:** 2861–2873.

Mullen, R.T., Lee, M.S., and Trelease, R.N. (1997). Identification of the peroxisomal targeting signal for cottonseed catalase. Plant J. **12:** 313–322.

Patel, S., and Dinesh-Kumar, S.P. (2008). *Arabidopsis* ATG6 is required to limit the pathogen-associated cell death response. Autophagy **4:** 20–27.

Queval, G., Issakidis-Bourguet, E., Hoeberichts, F.A., Vandorpe, M., Gakière, B., Vanacker, H., Miginiac-Maslow, M., Van Breusegem, F., and Noctor, G. (2007). Conditional oxidative stress responses in the *Arabidopsis* photorespiratory mutant cat2 demonstrate that redox state is a key modulator of daylength-dependent gene expression, and define photoperiod as a crucial factor in the regulation of H2O2-induced cell death. Plant J. **52:** 640–657.

Schmid, M., Davison, T.S., Henz, S.R., Pape, U.J., Demar, M., Vingron, M., Schölkopf, B., Weigel, D., and Lohmann, J.U. (2005). A gene expression map of *Arabidopsis thaliana* development. Nat. Genet. **37:** 501–506.

Schneeberger, K., Ossowski, S., Lanz, C., Juul, T., Petersen, A.H., Nielsen, K.L., Jørgensen, J.-E., Weigel, D., and Andersen, S.U. (2009). SHOREmap: Simultaneous mapping and mutation identification by deep sequencing. Nat. Methods **6:** 550–551.

Shaner, N.C., Campbell, R.E., Steinbach, P.A., Giepmans, B.N.G., Palmer, A.E., and Tsien, R.Y. (2004). Improved monomeric red, orange and yellow fluorescent proteins derived from Discosoma sp. red fluorescent protein. Nat. Biotechnol. **22:** 1567–1572.

Svenning, S., Lamark, T., Krause, K., and Johansen, T. (2011). Plant NBR1 is a selective autophagy substrate and a functional hybrid of the mammalian autophagic adapters NBR1 and p62/SQSTM1. Autophagy **7:** 993–1010.

Thompson, A.R., Doelling, J.H., Suttangkakul, A., and Vierstra, R.D. (2005). Autophagic nutrient recycling in Arabidopsis directed by the ATG8 and ATG12 conjugation pathways. Plant Physiol. **138:** 2097–2110.

Tognetti, V.B., et al. (2010). Perturbation of indole-3-butyric acid homeostasis by the UDP-glucosyltransferase UGT74E2 modulates *Arabidopsis* architecture and water stress tolerance. Plant Cell **22:** 2660–2679.

Van Breusegem, F., and Dat, J.F. (2006). Reactive oxygen species in plant cell death. Plant Physiol. **141:** 384–390.

Vandenabeele, S., Vanderauwera, S., Vuylsteke, M., Rombauts, S., Langebartels, C., Seidlitz, H.K., Zabeau, M., Van Montagu, M., Inzé, D., and Van Breusegem, F. (2004). Catalase deficiency drastically affects gene expression induced by high light in *Arabidopsis thaliana*. Plant J. **39:** 45–58.

Wang, W., Barnaby, J.Y., Tada, Y., Li, H., Tör, M., Caldelari, D., Lee, D.U., Fu, X.-D., and Dong, X. (2011). Timing of plant immune responses by a central circadian regulator. Nature **470:** 110–114.

Weaver, L.M., Gan, S., Quirino, B., and Amasino, R.M. (1998). A comparison of the expression patterns of several senescence-associated genes in response to stress and hormone treatment. Plant Mol. Biol. **37:** 455–469.

Winter, D., Vinegar, B., Nahal, H., Ammar, R., Wilson, G.V., and Provart, N.J. (2007). An "Electronic Fluorescent Pictograph" browser for exploring and analyzing large-scale biological data sets. PLoS ONE **2:** e718.

Yoshimoto, K., Jikumaru, Y., Kamiya, Y., Kusano, M., Consonni, C., Panstruga, R., Ohsumi, Y., and Shirasu, K. (2009). Autophagy negatively regulates cell death by controlling NPR1-dependent salicylic acid signaling during senescence and the innate immune response in *Arabidopsis*. Plant Cell **21:** 2914–2927.

Zhou, J., Wang, J., Cheng, Y., Chi, Y.-J., Fan, B., Yu, J.-Q., and Chen, Z. (2013). NBR1-mediated selective autophagy targets insoluble ubiquitinated protein aggregates in plant stress responses. PLoS Genet. **9:** e1003196.